Experimental testing of ab initio potential energy surfaces: Stereodynamics of NO(A2+) + Ne inelastic scattering at multiple collision energies

Supplementary Material For

'Experimental testing of ab initio potential energy surfaces: Stereodynamics of NO($A^2\Sigma^+$) + Ne inelastic scattering at multiple collision energies'

Thomas F. M. Luxford,[1] Thomas R. Sharples,[1] Kenneth G. McKendrick[1] and Matthew. L. Costen[1,a]

[1]*Institute of Chemical Sciences, Heriot-Watt University, Edinburgh, EH14 4AS, U. K.*

I. Determination of molecular beam speed distributions

The mean speeds of the molecular beams were obtained through direct analysis of the experimental images. The mean speeds of the NO/Ar and NO/He molecular beams were determined using the method described in our previous papers on NO(A) + Ar and NO(A) + He/D_2 scattering.[1, 2] This involved the fitting of a 2D Gaussian function to the beamspot in the background images, which results from the non-resonant 532 nm 2-photon ionization of unscattered NO(A) in the molecular beam. The distance, in pixels, of the mean position of the beamspot from the pixel defined as zero lab-frame velocity in the plane of the detector was recorded and converted into a velocity using the known pixel-to-velocity ratio.[2] A related method was used to determine the mean speed of the Ne molecular beam. A 2D Gaussian function was fitted to a non-resonant beamspot that appeared in the experimental images. This resulted from trace NO contamination of the pulsed valve backing lines that was unintentionally seeded in the Ne molecular beam during the experiment. Fig. S1 shows a single measurement scattering image for product state $N' = 9$ at $\langle E_{col} \rangle = 523$ cm^{-1}, in which the Ne beamspot is visible as a faint, isolated spot above and clearly separated from the intense scattering signal. The spread of speeds of the molecular beams in each case was assumed to be the same as that determined using a separate pulsed tagging and laser-induced-fluorescence probing time-of-flight method, which was described in detail in a previous publication.[1]

[a] Author to whom correspondence should be addressed. Electronic mail: m.l.costen@hw.ac.uk

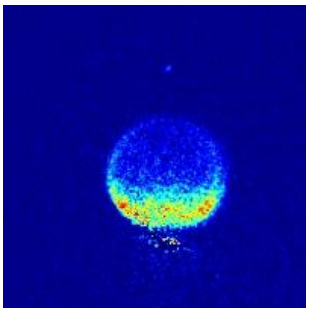

Fig. S1. Single acquisition experimental image for the inelastic collision of NO(A) with Ne at $\langle E_{col} \rangle$ = 523 cm^{-1}, for product state N' = 9. A faint beamspot, corresponding to the velocity of the Ne molecular beam is seen vertically displaced from the scattering signal.

II. Implementation of fitting constraints on the alignment moments

As discussed in the main text, the values of the alignment moments, $A_0^{\{2\}}$, $A_{1+}^{\{2\}}$ and $A_{2+}^{\{2\}}$ are restricted at scattering angles $\theta = 0$ and 180°. $A_0^{\{2\}}$ must tend to the extreme negative limit, $A_0^{\{2\}} = -1$, as a result of angular momentum conservation as **k** and **k'** become parallel or antiparallel. $A_{1+}^{\{2\}}$ and $A_{2+}^{\{2\}}$ must tend to $A_{1+}^{\{2\}} = A_{2+}^{\{2\}} = 0$ by symmetry as the scattering plane to which they are referenced is ill-defined when **k** and **k'** become parallel or antiparallel. In fitting to extract the moments, these restrictions were enforced by placing additional constraints on the allowed values of the coefficients in the Legendre expansions of each alignment moment.

In fitting to extract the alignment moments, each moment $A_{q+}^{\{2\}}(\theta)$ is expressed as a linear combination of Legendre polynomials with expansion coefficients c_λ^q.

$$A_{q+}^{\{2\}}(\theta) = \sum_{\lambda=0}^{m_{2q}-1} c_\lambda^q P_\lambda\left(1 - \theta/90°\right) \qquad \text{S1}$$

The even- and odd-order Legendre polynomials $P_\lambda\left(1 - \theta/90°\right)$ are even and odd functions, respectively. At $\theta = 0°$ the even- and odd-λ functions both take values of 1, while at $\theta = 180°$ the even- and odd-λ functions take values of 1 and -1, respectively. The constraint that $A_0^{\{2\}}(\theta) = -1$ at 0° and 180° is therefore equivalent to requiring that the following two conditions are met,

$$\sum_{\lambda=0,2,4\ldots}^{m_{20}-1} c_\lambda^0 + \sum_{\lambda=1,3,5\ldots}^{m_{20}-1} c_\lambda^0 = -1 \quad \text{S2}$$

$$\sum_{\lambda=0,2,4\ldots}^{m_{20}-1} c_\lambda^0 - \sum_{\lambda=1,3,5\ldots}^{m_{20}-1} c_\lambda^0 = -1 \quad \text{S3}$$

These equations are satisfied when,

$$\sum_{\lambda=0,2,4\ldots}^{m_{20}-1} c_\lambda^0 = -1 \quad \text{S4}$$

$$\sum_{\lambda=1,3,5\ldots}^{m_{20}-1} c_\lambda^0 = 0 \quad \text{S5}$$

We choose to meet these conditions by restricting the values of the $\lambda = 0$ and 1 expansion coefficients to take values determined by the sums of all higher even- and odd- order expansion coefficients, respectively,

$$c_0^0 = -1 - \sum_{\lambda=2,4,6\ldots}^{m_{20}-1} c_\lambda^0 \quad \text{S6}$$

$$c_1^0 = -\sum_{\lambda=3,5,7\ldots}^{m_{20}-1} c_\lambda^0 \quad \text{S7}$$

Similarly, the constraints on the $A_{1+}^{\{2\}}(\theta)$ and $A_{2+}^{\{2\}}(\theta)$ moments are equivalent to requiring that,

$$\sum_{\lambda=0,2,4\ldots}^{m_{2q}-1} c_\lambda^q + \sum_{\lambda=1,3,5\ldots}^{m_{2q}-1} c_\lambda^q = 0 \quad \text{S8}$$

$$\sum_{\lambda=0,2,4\ldots}^{m_{2q}-1} c_\lambda^q - \sum_{\lambda=1,3,5\ldots}^{m_{2q}-1} c_\lambda^q = 0 \quad \text{S9}$$

These equations are satisfied when,

$$\sum_{\lambda=0,2,4\ldots}^{m_{2q}-1} c_\lambda^q = 0 \qquad \text{S10}$$

$$\sum_{\lambda=1,3,5\ldots}^{m_{2q}-1} c_\lambda^q = 0 \qquad \text{S11}$$

We choose to meet these conditions by restricting the values of the $\lambda = 0$ and 1 expansion coefficients to take values determined by the sums of all higher even- and odd- order expansion coefficients, respectively,

$$c_0^q = -\sum_{\lambda=2,4,6\ldots}^{m_{2q}-1} c_\lambda^q \qquad \text{S12}$$

$$c_1^q = -\sum_{\lambda=3,5,7\ldots}^{m_{2q}-1} c_\lambda^q \qquad \text{S13}$$

This reduces the number of fitted parameters for each alignment moment by two, consistent with the implementation of two constraints to each moment.

III. Effect of Neon isotopic masses on the scattering kinematics.

Neon has three stable isotopes, present in the typical samples in the following natural abundances: 20Ne (0.9048); ^{21}Ne (0.0027); ^{22}Ne (0.0925). Since the ^{21}Ne isotope is much rarer, in what follows we have only considered the more abundant ^{20}Ne and ^{22}Ne. The different masses lead to different scattering kinematics, with different center-of-mass velocities and different product NO scattering velocities. The effect on the Newton diagrams and on simulated images is shown in Fig. S2 for the $N' = 10$ product state at both $\langle E_{col} \rangle = 523$ cm^{-1} and $\langle E_{col} \rangle = 1309$ cm^{-1}. The simulated image for the ^{22}Ne collisions is clearly different from that for the ^{20}Ne collisions, particularly in the backward hemisphere. However, the spread of collision energies is too broad to resolve the scattering from the different isotopes directly, with the simulations assuming the natural isotopic abundances in Fig. S2(c) and S2(f) displaying only a slight broadening of scattering ring. Nevertheless, this broadening was visible in the data when compared to simulations involving only ^{20}Ne, and all experimental data was

therefore fitted using basis functions including both isotopes. The isotopic mass was included in the Monte-Carlo selection step, with a ^{20}Ne:^{22}Ne ratio of 0.9048:0.0925.

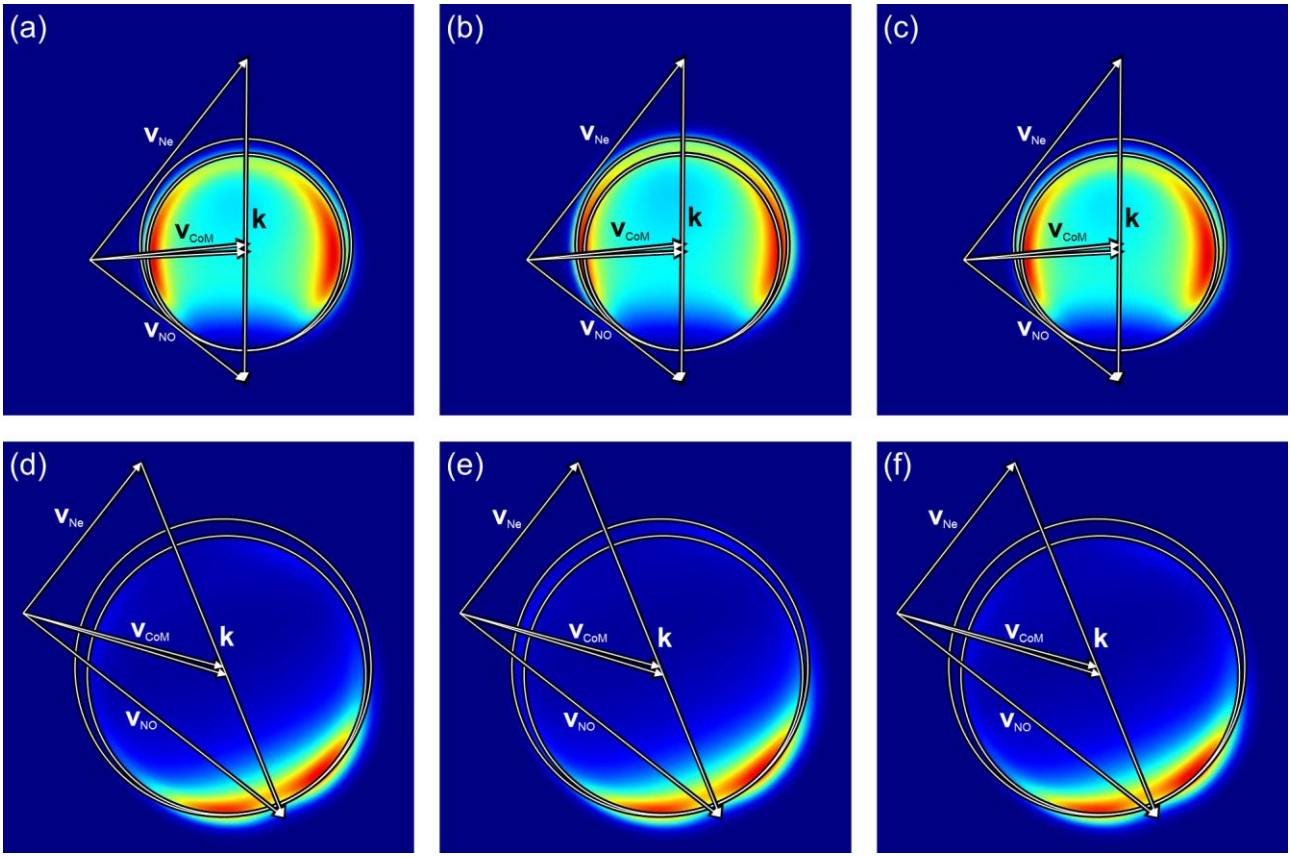

Fig. S2. V + H scattering images, simulated using the DCS and $A_{q+}^{\{2\}}(\theta)$ moments from quantum scattering calculations using the CF PES for $N' = 10$ for collisions of NO(A) with (a) ^{20}Ne at $\langle E_{col} \rangle$ = 523 cm^{-1}, (b) ^{22}Ne at $\langle E_{col} \rangle$ = 553 cm^{-1}, (c) ^{20}Ne at $\langle E_{col} \rangle$ = 523 cm^{-1} and ^{22}Ne at $\langle E_{col} \rangle$ = 553 cm^{-1} under natural isotopic abundances, (d) ^{20}Ne at $\langle E_{col} \rangle$ = 1309 cm^{-1}, (e) ^{22}Ne at $\langle E_{col} \rangle$ = 1384 cm^{-1}, (f) ^{20}Ne at $\langle E_{col} \rangle$ = 1309 cm^{-1} and ^{22}Ne at $\langle E_{col} \rangle$ = 1384 cm^{-1} under natural isotopic abundances. Overlaid are Newton diagrams showing the velocity vectors described in Fig. 1 of the main text for the collisions of NO(A) with both ^{20}Ne and ^{22}Ne.

References

1. T. R. Sharples, T. F. M. Luxford, D. Townsend, K. G. McKendrick, and M. L. Costen, J Chem Phys **143**, 204301 (2015).
2. T. F. M. Luxford, T. R. Sharples, D. Townsend, K. G. McKendrick, and M. L. Costen, J Chem Phys **145**, 084312 (2016).